ACS OMEGA

http://pubs.acs.org/journal/acsodf

Article

Novel Iron Oxide Nanoparticle-Fortified Carbon Paste Electrode for the Sensitive Voltammetric Determination of Atomoxetine

Hana M. Abumelha, Ali Q. Alorabi, Hussain Alessa, Nasser A. Alamrani, Arwa Alharbi, Ali A. Keshk, and Nashwa M. El-Metwaly*

Cite This: *ACS Omega* 2023, 8, 19006−19015

Read Online

ACCESS | Metrics & More | Article Recommendations | Supporting Information

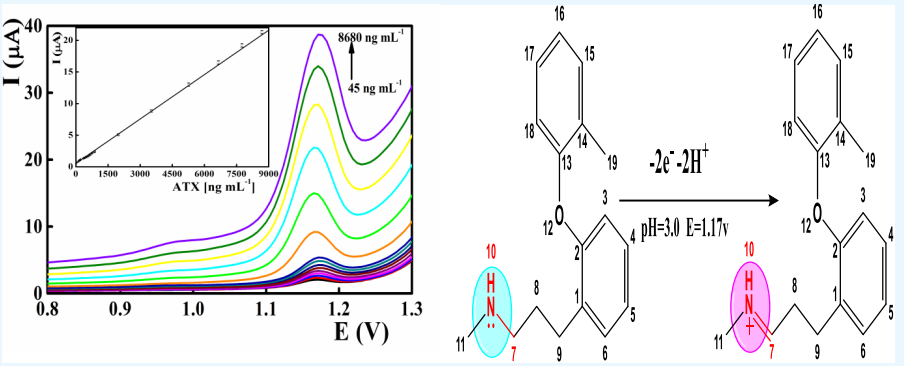

ABSTRACT: Herein, the fabrication and full characterization of a novel atomoxetine (ATX) voltammetric carbon paste electrode (CPE) fortified with iron oxide nanoparticles (FeONPs) is demonstrated. Modification of the carbon paste matrix with the metallic oxide nanostructure provides proper electrocatalytic activity against the oxidation of ATX molecules at the carbon paste surface, resulting in a noticeable improvement in the performance of the sensor. At the recommended pH value, ATX recorded an irreversible anodic peak at 1.17 V, following a diffusion-controlled reaction mechanism. Differential pulse voltammograms exhibited peak heights linearly correlated to the ATX content within a wide concentration range from 45 to 8680 ng mL^{-1}, with the limit of detection reaching 11.55 ng mL^{-1}. The electrooxidation mechanism of the ATX molecule was proposed to be the oxidation of the terminal amino group accompanied by the transfer of two electrons and two protons. The fabricated FeONPs/CPE sensors exhibited enhanced selectivity and sensitivity and therefore can be introduced for voltammetric assaying of atomoxetine-indifferent pharmaceutical and biological samples in the presence of its degradation products and metabolites.

1. INTRODUCTION

Depression represents a common chronic and often debilitating mental health condition that affects more than 10% of the general population,[1] with different symptoms including feelings of extreme sadness, mental confusion, and hopelessness. Antidepressants are classified into different categories based on the type of neurotransmitter and mechanism of action. Norepinephrine reuptake inhibitors (NRIs) selectively act on norepinephrine and epinephrine neurotransmitters through the inhibition of their reuptake into the brain cells and increasing their extracellular concentration, which in turn enhances neurotransmission.[2] Attention-deficit hyperactivity disorder (ADHD) is one of the chronic neurodevelopmental disorders with the core symptoms of inattention, impulsivity, and hyperactivity.[3−5] Atomoxetine (ATX) is one of the highly selective NRIs that blocks the noradrenaline transporter and enhances the dopamine and noradrenaline levels in the treatment of ADHD.[3,6−8] ATX is rapidly absorbed and principally metabolized into its 4-hydroxy (4-HATX) derivative and *N*-desmethylatomoxetine (*N*-DATX).[9−11] Several side effects have been reported for ATX, including adverse behavioral changes, headaches, sleep disorders, loss of appetite, and allergic reactions. In addition, more severe side effects consist of an increased risk of "suicidal thoughts," and cases of lethal poisoning with chronic overdose by ATX have been registered.[12] NRIS administration and usage has increased significantly over the last few decades and is recorded as the third most prescribed drug class in the USA.[13] Based on the above considerations, reliable analytical approaches are encouraged for monitoring trace residues of ATX in biological fluids and bulk pharmaceutical formulations. In addition, both

Received: March 14, 2023
Accepted: May 9, 2023
Published: May 18, 2023

the parent compound and its metabolites contribute to the therapeutic and toxic effects.

Several analytical approaches have been developed for monitoring ATX and its metabolite residues in pharmaceutical and biological samples, including chromatographic, spectrophotometric, and electrometric methods. Liquid chromatographic separation methods are useful and more popular for the sensitive and selective separation of ATX in complex matrices. High-performance liquid chromatography (HPLC) methods with UV[14,15] and fluorescence[16,17] detectors have been reported for the quantification of ATX in human plasma. Reversed-phase high-performance liquid chromatography (RP-HPLC) methods have been developed and validated for the quality control of ATX formulations.[18−20] Chromatography-tandem mass spectrometry approaches have been described for the simultaneous determination of ATX and its metabolites in human urine and plasma for the pharmacokinetic studies of ATX.[21−23] Because of the time-consuming nature and several derivatization processes associated with chromatographic methods, spectrophotometric methods can be the alternative choice for routine pharmaceutical analysis. Sensitive UV spectrophotometric methods,[24] oxidative coupling of atomoxetine with brucine,[25] and fluorimetric approaches[26] have also been reported in the literature.

Electroanalytical methods offer the advantages of a relatively short analysis time, simple pretreatment steps with simple equipment, and suitability for monitoring many pharmaceutical compounds.[27−30] Electrochemical sensors can be combined with other analytical approaches for monitoring pharmaceutical residues in drug formulations and biological samples. Moreover, the exploration of the electrooxidation behavior of the pharmaceutical compound molecules may explain the pharmacological activity, in vivo redox processes, and metabolic pathway. Regarding the electrometric approaches for ATX, carbon paste electrodes (CPEs) integrated with the ATX−tetraphenylborate ion pair decorated with TiO_2 nanoparticles were selected for the sensitive potentiometric determination of ATX.[31] The cited sensors showed a near Nernstian slope over a wide concentration range from 10^{-6} to 10^{-2} mol L^{-1}. Based on the electrochemical activity and the presence of oxidizable groups in ATX molecules, voltammetric measurement can be a feasible technique with excellent sensitivity, enhanced selectivity, and easier sample preparation. In this regard, differential pulse voltammetric methods were reported for ATX based on a glassy carbon electrode (GCE) and screen-printed sensors chemically coated with a boron-doped diamond layer (SP/BDDE) with limits of detection of 6.9×10^{-5} and 3.7×10^{-8} mol L^{-1}, respectively.[32,33]

With the aim of improved performance and sensitivity, studies were carried out through the integration of the matrix of a voltammetric sensor with different metal oxide nanoparticles.[34−44] Nanostructure-based sensors introduced different opportunities and improved the prospects of the analytical approach with enhanced sensitivity and selectivity. Based on the electrocatalytic activity of the electrode modifier, a noticeable shift in the redox potential and acceleration of the electron-transfer kinetics were reported. In the present work, the electroanalytical prospects of a novel carbon paste working sensor fortified with iron oxide nanoparticles were characterized for sensitive voltammetric assaying of atomoxetine in commercial pharmaceutical formulations and biological samples. The impacts of different electroanalytical parameters, including the electrode modifier, supporting electrolyte, scan rate, and reaction mechanism, were evaluated.

2. EXPERIMENTAL SECTION

2.1. Reference Drug and Reagents. Atomoxetine hydrochloride standard reference material (ATX, R-*N*-methyl-3-(*o*-tolyloxy)-3-phenylpropylamine hydrochloride, $C_{17}H_{21}NO$, 255.36 g mol^{-1}) was purchased from Sigma-Aldrich (CAS number 83015-26-3). The ATX stock solution was prepared by dissolving an appropriate amount of ATX in bidistilled water and stored at 4 °C. Paraffin oil (PO, Sigma) and graphite powders (1−2 μm, Aldrich) were used for the fabrication of the paste matrix. The metal oxide nanoparticles applied as electrode modifiers were zinc oxide nanopowder (Sigma-Aldrich), iron oxide nanoparticles (Sigma-Aldrich), and copper oxide nanopowder (Alfa Aesar). The universal buffer was applied as the supporting electrolyte, where sodium hydroxide solution was used to adjust the pH.

2.2. Working Electrodes and Measuring Apparatus. Cyclic and differential pulse voltammetric measurements were performed using a fully automated 797 VA Metrohm workstation (Metrohm, Switzerland). A 15 mL thermostated measuring cell was equipped with a three-electrode system composed of silver/silver chloride as the reference electrode, a platinum wire as the auxiliary electrode, and carbon paste as the working electrode. The carbon paste matrix was prepared by blending 80 μL of PO with 200 mg of graphite powder. The resulting homogeneous paste was packed into the electrode holder, and the electrode surface was regenerated as described elsewhere.[45] The nanostructure-integrated carbon paste was constructed in the same way by replacing 10 mg of the graphite powder with a metal oxide nanopowder.

2.3. Analytical Procedures. The measuring cell containing 10 mL of the supporting electrolyte at pH 3.0 was spiked with gradual increments of the ATX standard solution, and the DPVs were recorded applying the following electroanalytical conditions: pulse width 100 ms, pulse height 50 mV, and pulse duration 40 ms, with a scan rate of 60 mV s^{-1}. For each increment, the peak current (applying baseline correction) was plotted against the ATX concentration.

2.4. Degradation Studies. For oxidation stress studies, the stock ATX authentic solution (100 μg mL^{-1}) was prepared by dissolving the appropriate amount of ATX in a 3% H_2O_2 solution and refluxed for 3 h at room temperature. For hydrolysis studies, ATX was refluxed in 0.1 mol L^{-1} HCl/NaOH solutions for 3 h, and the degradation process was followed spectrophotometrically at 270 nm. The resulting degradation solutions were neutralized and evaporated till dryness. The solid residues were extracted with methanol to remove NaCl, filtered, and diluted to the appropriate concentration with methanol to obtain the stock solution for each degradation product.[19]

Moreover, the ATX pharmaceutical capsule powder was heated in a drying oven at 50 °C for 7 h; a suitable amount of the capsule powder equivalent to 10 mg of ATX was dissolved in water (final concentration 100 μg mL^{-1}) and assayed voltammetrically according to the official method. The aqueous solutions of the authentic ATX sample (100 μg mL^{-1}) and capsule solutions were irradiated (UV radiation at 30 °C for 12 h) to study the impact of UV radiation on the degradation of ATX in solutions.

2.5. Analysis of ATX Samples. The atomoxetine pharmaceutical sample (Atomox apex, 40 mg g^{-1} ATX gelatin

https://doi.org/10.1021/acsomega.3c01726
ACS Omega 2023, 8, 19006−19015

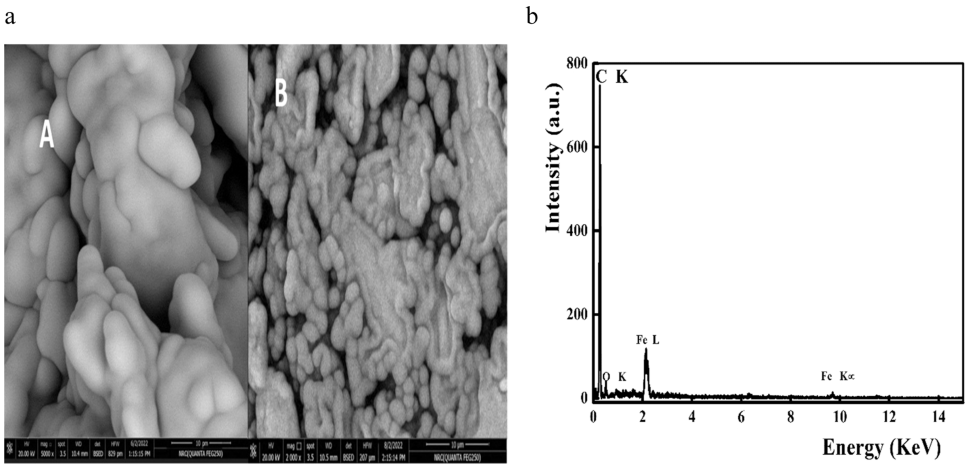

Figure 1. (a) Scanning electron microscopy images of bare carbon paste and FeONPs/CPE. (b) Energy-dispersive X-ray (EDX) spectrum of FeONPs/CPE.

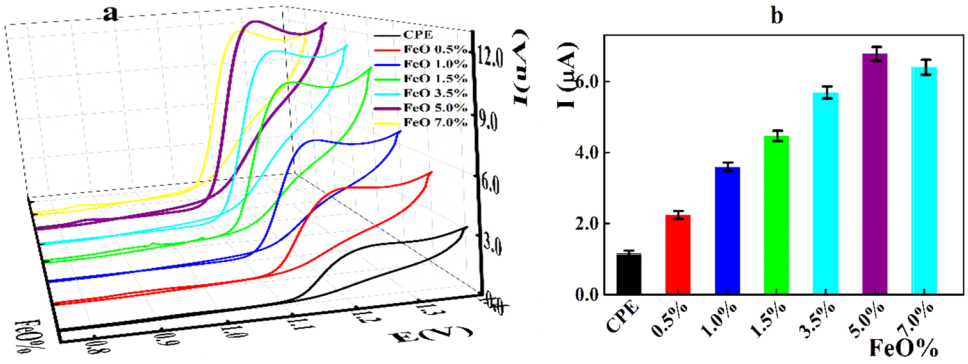

Figure 2. (a) Cyclic voltammograms (CVs) recorded in the presence of 5.2 μg mL^{-1} ATX applying carbon paste electrodes fortified with different FeONP ratios. (b) Peak currents for sensors fortified with different FeONPs ratios. Scan rate 60 mV s^{-1} at pH 3.0.

capsules, MULTI-Apex Pharma Company, New Cairo, Egypt) was purchased from the local market. Based on the manufacturer's specifications, the following inactive ingredients were present in the pharmaceutical sample: starch, gelatin, dimethicone, sodium lauryl sulfate, and titanium dioxide. Ten units of ATX capsules were separately weighed, emptied, and their contents crushed to furnish a homogeneous powder. A quantity equivalent to one capsule was dissolved in water, and further serial dilutions were carried out and analyzed according to the official method in comparison with the present voltammetric method.

Drug-free human plasma samples were centrifuged for 10 min at 5000 rpm and frozen at −20 °C till analysis. The frozen samples were allowed to thaw at room temperature, spiked with known desired quantities of the standard ATX stock solutions, vigorously shaken, and treated with methanol to remove the plasma proteins. The precipitated proteins were separated by centrifugation for 10 min at 4 °C. After dilution to the appropriate ATX concentration, the clear supernatant was analyzed according to the presented method. Samples of urine were laced with known increments of the standard ATX solution, mixed with methanol to remove residual sample protein, and the ATX content was assayed as usual.

3. RESULTS AND DISCUSSION

3.1. Morphological Characterization of FeONP-Integrated Carbon Paste Electrodes. Scanning electron microscopy (SEM) of both the bare carbon paste matrix and those fortified with iron oxide nanoparticles reveals a highly porous surface structure with a high degree of surface roughness (Figure 1a).[46,47] Iron oxide nanoparticles were dispersed within the paste matrix and strongly attached onto the graphite nanosheets with improved homogeneity of the paste. Moreover, FeONPs were uniformly distributed on the paste surface, with the particle size in the nanometer range. SEM images also show that the nanoparticles are well-adhered to the electrode, ensuring a consistent performance of the modified carbon paste electrode.[46,48]

Moreover, energy-dispersive X-ray (EDX) spectroscopy of the carbon paste matrix integrated with FeONPs confirmed the presence of iron oxide nanoparticles at the electrode surface. The EDX spectra distinctly showed four main peaks, which represent the elements carbon, oxygen, and iron. The relative intensity of each peak indicates the relative amount of each element present in the electrode matrix. As depicted, the C peak is the highest, indicating the higher concentration of carbon present in the electrode (graphite and pasting liquid). In addition, the EDX spectra also reveal the presence of other elements, such as silicon and calcium, which are likely present as impurities in the graphite powder or pasting liquid used for the formulation of the paste matrix. The SEM images and EDX spectra indicated that the electrode surface is coated with a layer of FeONPs with consistent properties. EDX spectroscopy can confirm the composition of the electrode surface, which further supports the homogeneity of the electrode matrix.

https://doi.org/10.1021/acsomega.3c01726
ACS Omega 2023, 8, 19006−19015

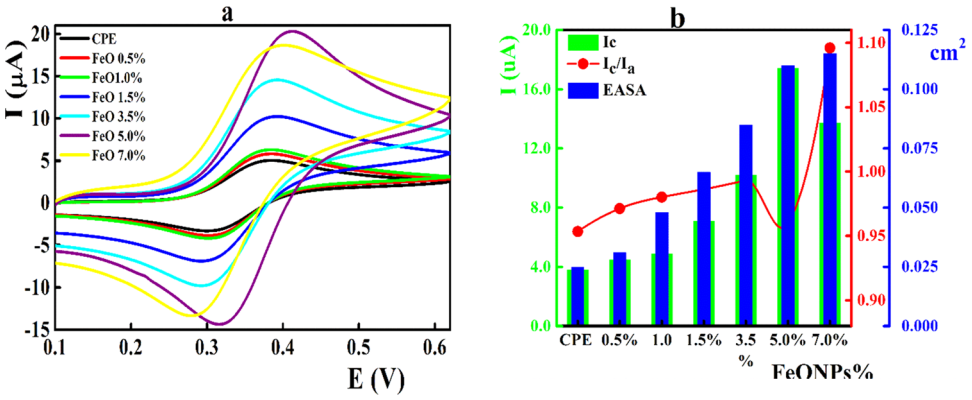

Figure 3. (a) Cyclic voltammograms (CVs) recorded for the 5.0×10^{-3} mol L^{-1} $[Fe(CN)_6]^{3-/4-}$ redox couple applying carbon sensors fortified with FeONPs; (b) values of the peak current of anodic and cathodic peaks and electroactive surface area (EASA) recorded at different FeONP ratios.

Table 1. Redox Characteristics of the Recorded Cyclic Voltammograms and Electroactive Surface Areas (EASAs) at Different FeONP/CPE ratios

electrode	E_{pa} (V)	E_{pc} (V)	ΔE (V)	I_{pa} (A)	I_{pc} (A)	I_{pc}/I_{pa} (A)	active area (cm^2)
CPE	0.380	0.308	0.072	3.8×10^{-6}	-3.62×10^{-6}	−0.95349	0.025
FeO 0.5%	0.380	0.308	0.072	4.5×10^{-6}	-4.37×10^{-6}	−0.97131	0.031
FeO 1.0%	0.381	0.305	0.076	4.88×10^{-6}	-4.78×10^{-6}	−0.98021	0.048
FeO 1.5%	0.380	0.308	0.072	7.1×10^{-6}	7.1×10^{-6}	−0.98627	0.065
FeO 3.5%	0.386	0.302	0.084	1.02×10^{-5}	-1.01×10^{-5}	−0.99303	0.085
FeO 5%	0.403	0.326	0.077	1.74×10^{-5}	-1.67×10^{-5}	−0.95977	0.110
FeO 7.5%	0.392	0.290	0.102	1.37×10^{-5}	-1.29×10^{-5}	−1.09602	0.115

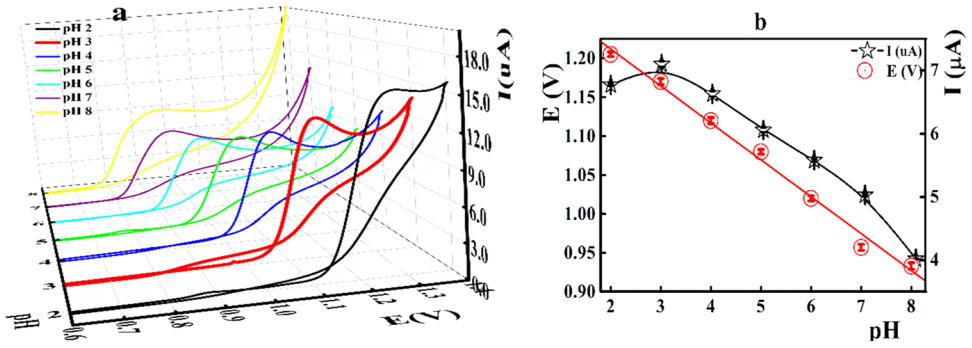

Figure 4. (a) CVs recorded in the presence of 5.2 μg mL^{-1} ATX at different pH values. (b) Peak currents and peak potentials registered against pH values of the supporting electrolyte.

3.2. Electrochemical Behavior of ATX at the FeONP-Integrated Sensors. A careful survey of the literature indicated no reported studies on the electrochemical behavior of ATX at the carbon paste electrodes, as previous voltammetric studies were carried out at GCEs and SP/BDDEs, respectively.[32,33] Therefore, the present study explored the electrochemical behavior of ATX molecules at the bare carbon paste electrodes and those modified with different metal oxide nanoparticles (Figure S1). At the bare carbon paste electrode surface, ATX recorded a single broad irreversible oxidation peak at 1.25 V with a limited peak height. Based on the electrocatalytic activity of different metallic nanoparticles, the recorded peak current was gradually enhanced to its maximum value by the modification of nanostructures with FeONPs. Both copper oxide and zinc oxide nanoparticles exhibited relatively lower peak currents compared with FeONPs due to the difference in their overall redox potentials and bandgap values.

Next, carbon paste working electrodes fortified with different ratios of FeONPs were applied for the voltammetric determination of ATX (Figure 2). The peak heights were gradually improved based on the incorporation of the electrode matrix with FeONPs, with the maximum value at 5.0% FeONPs (about 5-fold amplification compared with the bare electrode). At a higher FeONP content, lower peak currents were achieved due to the change in paste properties and the requirement for additional amounts of paraffin oil.

The electrochemical behavior of the constructed sensors integrated with the iron oxide nanostructure was explored in a ferricyanide (FCN) solution. The peak heights were gradually improved via modification with FeONPs based on their electrocatalytic activity and enhancement of the electron-transfer process (Figure 3 and Table 1). Cyclic voltammograms recorded at the bare carbon paste showed an anodic peak current (I_{pa}) value of 3.8 μA; next, the I_{pa} values were enhanced to 7.1, 10.2, and 17.4 μA for 1.5, 3.5, and 5.0%

https://doi.org/10.1021/acsomega.3c01726
ACS Omega 2023, 8, 19006−19015

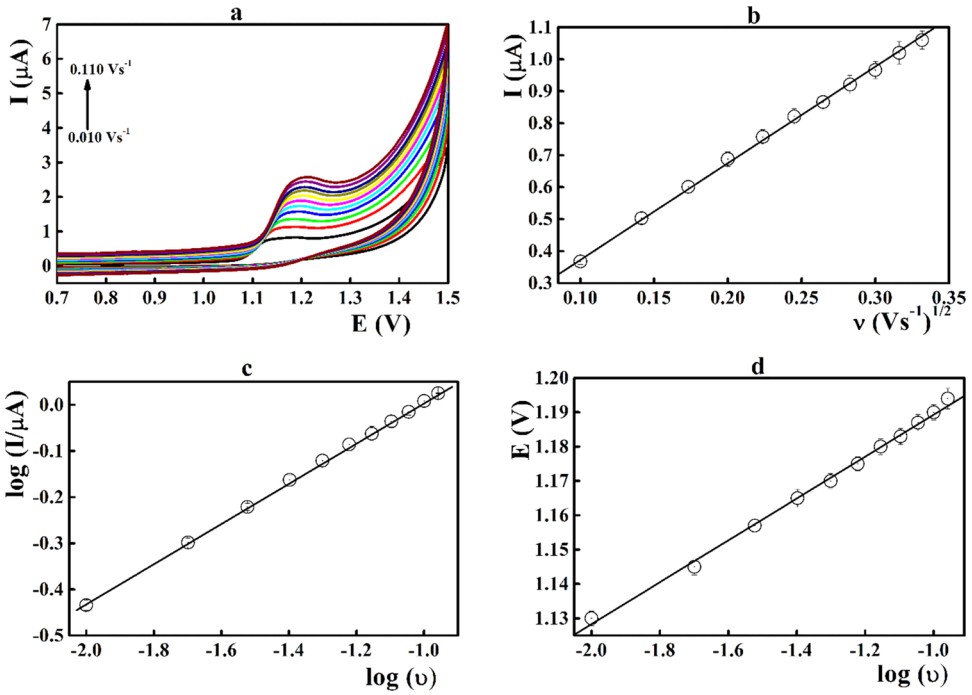

Figure 5. (a) Recorded CVs for 3.0 μg mL^{-1} ATX at different scan rates; (b) values of the peak current at different scan rates against the square root of the scan rate; (c) estimated logarithmic value of the peak current at different scan rates against the logarithmic value of the corresponding scan rate; and (d) the recorded peak potential against the logarithmic value of the scan rate.

FeONPs, respectively. The highest performance was recorded for sensors incorporated with 5.0% FeONPs, confirming the role of FeONPs in the improvement of the electron-transfer process and sensor performance.

To estimate the electroactive surface area (EASA) of the integrated carbon paste electrodes, CVs were recorded in the FCN redox couple, applying different scan rates. The estimated peak currents were linearly correlated to the square root values of the scan rate [ν (V s^{-1})]$^{1/2}$, confirming the diffusion-controlled mechanism of FCN at the electrode surface. The EASA for each electrode was calculated following the Randles−Sevik equation.[49,50] The estimated EASA values were enhanced from 0.025 to 0.115 cm^2 for the bare and 7.0% FeONP carbon paste electrodes, respectively.

3.3. Dependence on pH. The nature and pH value of the supporting electrolyte controlled the course of the ongoing electrochemical behavior of the oxidizable analyte and, subsequently, the shape and peak current of the recorded voltammograms. As illustrated in Figure 4a, the recorded CVs at 5.0% FeONPs/CPE in BR buffer with different pH values were pH dependent. The oxidation peaks were shifted toward the negative direction by increasing the pH values, sustaining the involvement of hydrogen protons in the electrode reaction.[50] The peak potential was linearly correlated to the pH value as follows: $E_{P(V)} = -0.0474 \pm 0.0012$ pH + 1.3067 (r = −0.9957), with a near Nernstian slope value. Therefore, it can be concluded that an equal number of electrons and protons were involved in the electrode reaction. The obtained slope value disagrees with the previously published ATX voltammetric methods.[32,33]

In addition, the recorded CVs registered the maximum peak current value at pH 3.0, which continuously decreased at higher pH values; therefore, voltammetric analysis of ATX will be carried out at pH 3, which is close to the optimum pH in the case of previous ATX sensors.[33]

3.4. Electrochemical Behavior at Different Scan Rates. Cyclic voltammograms for ATX at FeONPs/CPE recorded at different scan rates offer more insights into the electrochemical behavior of ATX molecules at the FeONPs/CPE surface and the number of electrons transferred.[50] As illustrated in Figure 5a, CVs for ATX molecules were scanned over a wide scan rate ranging from 0.010 to 0.110 V s^{-1} (Figure 5a). The estimated peak currents increased with the scan rate, and the oxidation peak potentials were shifted toward the positive direction, indicating the irreversibility of the electrooxidation of ATX molecules. Plotting the peak current against the square root of the scan rate ([ν (V s^{-1})]$^{1/2}$) revealed a typically linear relationship (r = 0.9995), confirming the irreversibility of the electrooxidation process at the electrode surface (Figure 5b). Next, the logarithmic value of the recorded peak current showed a linear equation against the corresponding logarithmic value of the scan rate (log ($I_{\mu A}$) = 0.43935 log υ (V s^{-1}) + 0.44675; r = 0.9998) (Figure 3c). The slope value was close to the theoretical value (0.5) for the diffusion-controlled reaction,[51,52] which is in agreement with the ATX behavior at GCE and SP/BDDE.[32,33]

Eventually, the potential values were shifted toward the positive direction following a linear relationship with the logarithmic value of the scan rate (E_{pV} = 0.0610 log υ (V s^{-1}) + 1.2503; r = 0.9986, Figure 5d). Based on the Laviron equation,[53] two electrons participated in the electrooxidation of the ATX molecule at the FeONPs/CPE compared with four electrons on GCE and SP/BDDE.[32,33]

The reported oxidation pathway of the ATX molecule involved a multistep oxidation process with the formation of the corresponding aldehyde and amine derivatives with the involvement of four electrons and four protons.[32] Herein, based on the present scan rate and pH studies, the oxidation of the ATX molecule includes the transfer of only two electrons and two protons. In addition, molecular orbital calculations

https://doi.org/10.1021/acsomega.3c01726
ACS Omega 2023, 8, 19006−19015

Scheme 1. Proposed Oxidation Mechanism of the Atomoxetine Molecule at the FeONP-Integrated Sensor

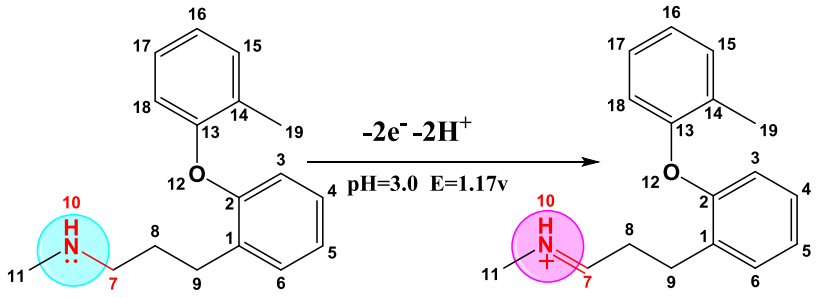

performed on atomoxetine molecules (Tables S1, S2, and Figure S2) indicated the highest electron density at nitrogen,[54] and the postulated redox mechanism is displayed in Scheme 1.

3.5. Linear Range and Analytical Parameters. At the optimized measuring conditions, the electroanalytical performance of the fabricated carbon paste sensors was validated. The peak current values of the recorded differential pulse voltammograms were plotted against the corresponding ATX concentrations (Figure 6 and Table 2). The constructed

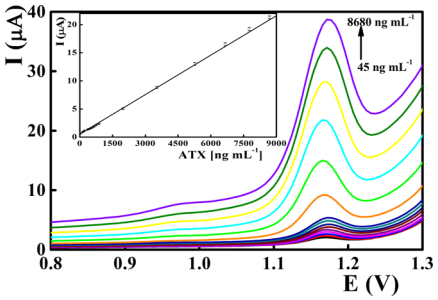

Figure 6. Differential pulse voltammetric determination of atomoxetine at FeONPs/CPE.

Table 2. Electroanalytical Performance of FeONPs/CPE Atomoxetine Sensors[a]

parameters	
peak potential (V)	1.17
measuring pH	3.0
linear range (ng mL^{-1})	45−8680
slope (μA mL^{-1} ng^{-1})	0.003
SD of slope (μA $mL^{-1}ng^{-1}$)	4.7×10^{-5}
intercept (μA cm^{-2})	0.4257
SD of intercept (μA cm^{-2})	0.0105
multiple *R*	0.9999
R square	0.9995
repeatability	0.55
intermediate precision	1.22
RSD %	1.83
LOD (ng mL^{-1})	11.55
LOQ (ng mL^{-1})	35

[a]Average of five experiments.

calibration graphs were linear (r = 0.9999) within a wide concentration range from 45 to 8680 ng mL^{-1}. The estimated values of the limit of quantification (LOQ) and limit of detection (LOD) were 35.0 and 11.55 ng mL^{-1}, respectively.[55,56]

Compared with the previously reported ATX voltammetric methods based on GCE and SP/BDDE as working electrodes,[32,33] the present FeONPs/CPE showed improved sensitivity over a wide linear range. Moreover, the simple fabrication protocol with a prolonged lifetime indicates a promising future of the presented sensors compared with SP/BDDE sensors (Table S3). Moreover, compared with chromatographic and spectrophotometric techniques, electrometric approaches show a short analysis time, avoid exposure to hazardous organic solvents, and involve low instrumentation.

The repeatability and stability of the DPVs were evaluated over a prolonged operation period. After continuous operation for 28 days, the peak performance remains constant, with 94.69% of the original peak, which then diminished to reach about 88.8% after 60 days (Figure S3).

3.6. Specificity of the Method. Drug additive and degradation profiling involves the study and quantification of the degradation products and various impurities in bulk drug materials and pharmaceutical formulations. Nowadays, monitoring of such contaminants represents one of the most crucial considerations in the pharmaceutical industry. Analytical approaches applied for the determination of active pharmaceutical compounds and formulations represent an integral part of the quality-by-design concept that is recommended in the ICH Guideline.[57,58] However, many of the unidentified impurities are potential health hazards, and therefore, to ensure the safety of a pharmaceutical formulation, the identification of degradants and impurities should be taken into consideration for a new analytical approach.[57−60] Moreover, the pharmaceutical formulation should show adequate stability throughout its shelf life with respect to its purity, identity, and quality. However, forced degradation studies provide information to support the identification of degradation pathways and possible degradants. This type of holistic consideration of the nature and fate of impurities is considered a key piece of the overall analytical control strategy.

Herein, ATX was exposed to hydrolytic and forced degradation studies as described elsewhere.[19,61] Forced degradation studies of ATX solution indicated the degradation of about 25% ATX when refluxed in an acidic medium after 1 h, while complete degradation was recorded after 3 h. A similar degradation rate was monitored in an alkaline medium. Oxidative stress degradation resulted in the degradation of 32% of the initial ATX. Considering the thermal degradation of ATX, about 12−15% of the initial ATX was degraded after heating for 1 h, with complete degradation after contentious heating for 7 h. In contrast, negligible photolytic degradation (<2%) was recorded for the ATX capsule irradiated with UV light for 2 days. Voltammetrically, the ATX acidic degradants recorded DPVs with the appearance of a new signal at about 0.85 V, which did not interfere with the primary atomoxetine

https://doi.org/10.1021/acsomega.3c01726
ACS Omega 2023, 8, 19006−19015

Table 3. Voltammetric Determination of Atomoxetine in Pharmaceutical and Biological Samples

sample	added (ng mL^{-1})	found (ng mL^{-1})	bias %[aa]	recovery (%)	HPLC[aa]
atomox	150	148	1.33	98.67	100.51
	550	552	0.36	100.36	100.12
	1850	1860	0.54	100.54	99.94
	4500	4510	0.22	100.22	98.93
mean				99.95	99.88
variance				0.75	0.45
observations				4	4
df				3	3
t-test	0.45				
F-test[bb]	1.65				
t critical two-tail	2.45				
F critical one-tail	9.28				
sample	added (ng mL^{-1})	found (ng mL^{-1})	bias %	recovery (%)	HPLC[aa]
urine	50	49.8	0.40	99.60	100.61
	450	453	0.67	100.67	100.40
	750	752	0.27	100.27	99.98
	6650	6645	0.08	99.92	98.91
mean				100.11	99.98
variance				0.21	0.57
observations				4	4
df				3	3
t-test	0.38				
F[b]	2.73				
t critical two-tail	2.45				
F critical one-tail	9.28				
sample	added (ng mL^{-1})	found (ng mL^{-1})	bias %	recovery (%)[aa]	HPLC[aa]
serum	360	364	−1.11	101.11	100.05
	2900	2880	0.69	99.31	100.35
	6500	6520	−0.31	100.31	99.98
	7500	7525	−0.33	100.33	99.91
mean				100.27	99.90
variance				0.54	0.19
observations				4	4
df				3	3
t-test	0.38				
F[bb]	2.793231				
t critical two-tail	2.45				
F critical one-tail	9.28				

[a]Each result is an average of three determinations. [b]Tabulated *F* and *t* values at $p = 0.05$.

signal at 1.17 V (Figure S4). This can be attributed to the presence of a terminal amino group in the degradation products. For alkaline hydrolysis, UV irradiation, and thermolysis degradation, no obvious change in the ATX peak was observed, with a diminished peak height.

According to the manufacturer, some excipients are present in the commercial ATX pharmaceutical formulation, including corn starch and dimethicone. None of these additives showed noticeable interference with the atomoxetine signal. The aforementioned degradation and interference studies used the voltammetric approach for the selective quantification of atomoxetine in pharmaceutical formulations as the stability-indicating protocol without the necessity of pretreatment or separation steps.

3.7. Sample Analysis. After oral administration of ATX, it is converted into 4-hydroxy (4-HATX) and *N*-desmethylatomoxetine (*N*-DATX) as the main metabolites. Nearly all of the ATX metabolites are eliminated by excretion into urine within the first 24 h.[10] Both metabolites have nearly the chemical structure of the parent compound (Figure S5) and are expected to exhibit voltammograms similar to that of the ATX molecule. The molecular orbital calculations confirm the highest electron density at the nitrogen atom, similar to the parent compound; therefore, the presented approach is suitable for the quantification of ATX and its metabolites in biological fluids.

The presented iron oxide nanoparticle-integrated sensors exhibited enhanced sensitivity and selectivity toward ATX; therefore, their suitability for voltammetric assaying of ATX in biological samples and pharmaceutical formulations was tested. The analyzed samples were spiked with known ATX concentrations and analyzed according to the presented voltammetric method and HPLC-UV method at 270 nm. Acceptable recovery values with lower relative standard deviation values indicate the applicability of the proposed analysis protocol for the determination of atomoxetine (Table 3).

https://doi.org/10.1021/acsomega.3c01726
ACS Omega 2023, 8, 19006−19015

4. CONCLUSIONS

The present study investigated the construction and electrochemical prospects of a novel atomoxetine voltammetric analytical approach based on carbon paste sensors integrated with iron oxide nanoparticles. Based on the electrocatalytic activity of the FeONPs, the atomoxetine molecule was irreversibly oxidized following a diffusion-controlled reaction mechanism with the participation of two electrons/protons, as confirmed by molecular orbital calculation studies. Calibration graphs were linear within the ATX concentration range from 45 to 8680 ng mL^{-1}, with an LOD value of 11.55 ng mL^{-1}. Modification with FeONPs offers a sensitive and reliable voltammetric protocol for ATX in the presence of its degradants and metabolites and is explored for simple and reliable assaying of ATX in pharmaceutical and biological samples with acceptable average recoveries comparable to that of reported chromatographic methods. Compared with previously reported ATX voltammetric sensors, FeONPs/CPEs showed improved sensitivity, along with ease of fabrication and a prolonged operational lifetime.

■ ASSOCIATED CONTENT

Data Availability Statement

All relevant data are within the manuscript and available from the corresponding author upon request.

Supporting Information

The Supporting Information is available free of charge at https://pubs.acs.org/doi/10.1021/acsomega.3c01726.

Cyclic voltammograms recorded in the presence of 5.2 $\mu g\ mL^{-1}$ ATX at carbon paste sensors integrated with different metallic nanostructures (Figure S1); HOMO and LUMO structures of atomoxetine (Figure S2); differential pulse voltammograms of 6.0 $\mu g\ mL^{-1}$ ATX at FeONPs/CPE after different intervals (Figure S3) and in the presence of its degradation products (Figure S4); and electrochemical oxidation mechanism of atomoxetine metabolites on FeONPs/CPE at pH 3.5 (Figure S5); computed molecular orbital calculations of the atomoxetine molecule (Table S1) and 4-hydroxyatomoxetine metabolite (Table S2); comparison of different ATX sensors (Table S3); and computed molecular orbital calculations of the *N*-desmethylatomoxetine metabolite (Table S3) (PDF)

■ AUTHOR INFORMATION

Corresponding Author

Nashwa M. El-Metwaly − *Department of Chemistry, Faculty of Applied Sciences, Umm Al-Qura University, Makkah 24382, Saudi Arabia; Department of Chemistry, Faculty of Science, Mansoura University, Mansoura 35516, Egypt;* orcid.org/0000-0002-0619-6206; Email: n_elmetwaly00@yahoo.com, nmmohamed@uqu.edu.sa

Authors

Hana M. Abumelha − *Department of Chemistry, College of Science, Princess Nourah Bint Abdulrahman University, Riyadh 11671, Saudi Arabia*

Ali Q. Alorabi − *Department of Chemistry, Faculty of Sciences, Al-Baha University, Albaha 65799, Saudi Arabia*

Hussain Alessa − *Department of Chemistry, Faculty of Applied Sciences, Umm Al-Qura University, Makkah 24382, Saudi Arabia*

Nasser A. Alamrani − *Department of Chemistry, College of Science, University of Tabuk, Tabuk 71421, Saudi Arabia*

Arwa Alharbi − *Department of Chemistry, Faculty of Applied Sciences, Umm Al-Qura University, Makkah 24382, Saudi Arabia*

Ali A. Keshk − *Department of Chemistry, College of Science, University of Tabuk, Tabuk 71421, Saudi Arabia*

Complete contact information is available at: https://pubs.acs.org/10.1021/acsomega.3c01726

Notes

The authors declare no competing financial interest.

■ ACKNOWLEDGMENTS

The authors acknowledge the Princess Nourah bint Abdulrahman University Researchers Supporting Project Number PNURSP2023R22 and the Princess Nourah bint Abdulrahman University, Riyadh, Saudi Arabia.

■ REFERENCES

(1) Wong, E. H.; Sonders, M. S.; Amara, S. G.; Tinholt, P. M.; Piercey, M. F.; Hoffmann, W. P.; Hyslop, D. K.; Franklin, S.; Porsolt, R. D.; Bonsignori, A.; Carfagna, N.; McArthur, R. A. Reboxetine: a pharmacologically potent, selective, and specific norepinephrine reuptake inhibitor. *Biol. Psychiatry* **2000**, *47*, 818−829.

(2) Gasior, M.; Bergman, J.; Kallman, M. J.; Paronis, C. A. Evaluation of the reinforcing effects of monoamine reuptake inhibitors under a concurrent schedule of food and iv drug delivery in rhesus monkeys. *Neuropsychopharmacology* **2005**, *30*, 758−764.

(3) Biederman, J.; Faraone, S. V. Attention-deficit hyperactivity disorder. *Lancet* **2005**, *366*, 237−248.

(4) Bramham, J.; Murphy, D. G. M.; Xenitidis, K.; Asherson, P.; Hopkin, G.; Young, S. Adults with attention deficit hyperactivity disorder: an investigation of age-related differences in behavioural symptoms, neuropsychological function and co-morbidity. *Psychol. Med.* **2012**, *42*, 2225−2234.

(5) Goodman, D. W. *ADHD Neurobiologic Evidence and Diagnostic Nuances*; NEI Psychopharmacology Congress, 2015.

(6) Bymaster, F. P.; Katner, J. S.; Nelson, D. L.; Hemrick-Luecke, S. K.; Threlkeld, P. G.; Heiligenstein, J. H.; Morin, S. M.; Gehlert, D. R.; Perry, K. W. Atomoxetine increases extracellular levels of norepinephrine and dopamine in prefrontal cortex of rat: a potential mechanism for efficacy in attention deficit/hyperactivity disorder. *Neuropsychopharmacology* **2002**, *27*, 699−711.

(7) Witcher, J. W.; Long, A.; Smith, B.; Sauer, J. M.; Heilgenstein, J.; Wilens, T.; Spencer, T.; Biederman, J. Atomoxetine pharmacokinetics in children and adolescents with attention deficit hyperactivity disorder. *J. Child Adolesc. Psychopharmacol.* **2003**, *13*, 53−63.

(8) Yu, G.; Li, G. F.; Markowitz, J. S. Atomoxetine: a review of its pharmacokinetics and pharmacogenomics relative to drug disposition. *J. Child Adolesc. Psychopharmacol.* **2016**, *26*, 314−326.

(9) Ring, B. J.; Gillespie, J. S.; Eckstein, J. A.; Wrighton, S. A. Identification of the human cytochromes P450 responsible for atomoxetine metabolism. *Drug Metab. Dispos.* **2002**, *30*, 319−323.

(10) Sauer, J. M.; Ring, B. J.; Witcher, J. W. Clinical pharmacokinetics of atomoxetine. *Clin. Pharmacokinet.* **2005**, *44*, 571−90.

(11) Vijetha, K.; Ramu, A.; Vidyadhara, S.; Subbarao, J. Validated RP-HPLC and UV spectrophotometry method for the estimation of atomoxetine hydrochloride in pharmaceutical dosage forms. *Der Pharm. Lett.* **2015**, *7*, 92−97.

(12) Reed, V. A.; Buitelaar, J. K.; Anand, E.; Day, K. A.; Treuer, T.; Upadhyaya, H. P.; Coghill, D. R.; Kryzhanovskaya, L. A.; Savill, N. C.

The safety of atomoxetine for the treatment of children and adolescents with attention-deficit/hyperactivity disorder: a comprehensive review of over a decade of research. *CNS Drugs* **2016**, *30*, 603−628.
(13) Pratt, L. A.; Brody, D. J.; Gu, Q. *Antidepressant Use among Persons Aged 12 and Over: United States, 2011−2014*, NCHS Data Brief. Number 283; National Center for Health Statistics, 2017.
(14) Guo, W.; Li, W.; Guo, G.; Zhang, J.; Zhou, B.; Zhai, Y.; Wang, C. Determination of atomoxetine in human plasma by a high performance liquid chromatographic method with ultraviolet detection using liquid−liquid extraction. *J. Chromatogr. B* **2007**, *854*, 128−134.
(15) Teichert, J.; Rowe, J. B.; Ersche, K. D.; Skandali, N.; Sacher, J.; Aigner, A.; Regenthal, R. Determination of Atomoxetine or Escitalopram in human plasma by HPLC. Applications in Neuroscience Research Studies. *Int. J. Clin. Pharmacol. Ther.* **2020**, *58*, 426.
(16) Ulu, S. T. Sensitive high performance liquid chromatographic method for determination of atomoxetine in plasma and urine precolumn derivatization with 1-dimethylaminonaphthalene-5-sulphonyl chloride. *J. Liq. Chromatogr. Relat. Technol.* **2012**, *35*, 747−756.
(17) Stegmann, B.; Dörfelt, A.; Haen, E. Quantification of methylphenidate, dexamphetamine, and atomoxetine in human serum and oral fluid by HPLC with fluorescence detection. *Ther. Drug Monit.* **2016**, *38*, 98−107.
(18) Jagadeesh, B. V. V. S.; Raju, S. S.; Rao, V. J.; Rao, J. V. L. N. S. Reverse Phase HPLC Analysis of Atomoxetine in Pharmaceutical Dosage Forms. *Asian - J. Chem.* **2009**, *21*, 829−833.
(19) Patel, S. K.; Patel, N. J. Development and validation of a stability-indicating RP-HPLC method for determination of atomoxetine hydrochloride in tablets. *J. AOAC Int.* **2010**, *93*, 1207−1214.
(20) Lakshmi, G. T.; Rao, Y. S.; Rao, K.; Prasada, V.; Kumar, T. H. RP-HPLC Method for Estimation of Atomoxetine Hydrochloride in Bulk and Pharmaceutical Dosage Form. *Res. J. Pharm. Biol. Chem. Sci.* **2015**, *6*, 1208−1214.
(21) Mullen, J. H.; Shugert, R. L.; Ponsler, G. D.; Li, Q.; Sundaram, B.; Coales, H. L.; Yakupkovic, J. E.; LeLacheur, R. M.; Wheeler, W. J.; Belas, F. J.; Sauer, J. M. Simultaneous quantification of atomoxetine as well as its primary oxidative and O-glucuronide metabolites in human plasma and urine using liquid chromatography tandem mass spectrometry (LC/MS/MS). *J. Pharm. Biomed. Anal.* **2005**, *38*, 720−733.
(22) Papaseit, E.; Marchei, E.; Mortali, C.; Aznar, G.; Garcia-Algar, O.; Farrè, M.; Pacifici, R.; Pichini, S. Development and validation of a liquid chromatography−tandem mass spectrometry assay for hair analysis of atomoxetine and its metabolites: Application in clinical practice. *Forensic Sci. Int.* **2012**, *218*, 62−67.
(23) Choi, C. I.; Bae, J. W.; Lee, H. I.; Jang, C. G.; Sohn, U. D.; Lee, S. Y. Determination of atomoxetine metabolites in human plasma by liquid chromatography/tandem mass spectrometry and its application to a pharmacokinetic study. *J. Chromatogr. B* **2012**, *885−886*, 103−108.
(24) Reddy, D. S.; Yashaswini, E.; Kumar, A. A. A simple assay method development and validation of Atomoxetine hydrochloride in tablets by UV spectrophotometry. *Indo Amer. J. Pharm. Sci.* **2016**, *3*, 393−398.
(25) Raghubabu, K.; Shanti Swarup, L.; Ramu, B. K.; Rao, M. N. Simple and convenient visible spectrophotometric assay of atomoxetine hydrochloride in bulk drug and pharmaceutical preparations. *Int. J. Chem. Sci.* **2012**, *10*, 643−654.
(26) Derayea, S. M.; Omar, M. A.; Abu-Hassan, A. A. Studying the association complex formation of atomoxetine and fluvoxamine with eosin Y and its application in their fluorimetric determination. *R. Soc. Open Sci.* **2018**, *5*, No. 170943.
(27) Siddiqui, M. R.; AlOthman, Z. A.; Rahman, N. Analytical techniques in pharmaceutical analysis: A review. *Arab. J. Chem.* **2017**, *10*, S1409−S1421.
(28) Ozkan, S. A. *Electroanalytical Methods in Pharmaceutical Analysis and Their Validation*; HNB Publishing, 2012.
(29) Ozkan, S. A.; Kauffmann, J. M.; Zuman, P. *Electroanalysis in Biomedical and Pharmaceutical Sciences: Voltammetry, Amperometry, Biosensors, Applications*; Springer, 2015.
(30) Ziyatdinova, G.; Budnikov, H. Electroanalysis of antioxidants in pharmaceutical dosage forms: state-of-the-art and perspectives. *Monatsh. Chem.* **2015**, *146*, 741−753.
(31) Shawish, H. M. A.; Saadeh, S.; Tamous, H.; Saadeh, S. M.; Tbaza, A. Determination of atomoxetine hydrochloride in biological fluids using potentiometric carbon paste electrode modified by TiO2 nanoparticles. *Acta Chim. Slov.* **2018**, *65*, 811−822.
(32) Pérez-Ortiz, M.; Munoz, C.; Zapata-Urzúa, C.; Álvarez-Lueje, A. Electrochemical behavior of atomoxetine and its voltammetric determination in capsules. *Talanta* **2010**, *82*, 398−403.
(33) Šelešovská, R.; Navrátil, T.; Hrdlička, V.; Michniak, P.; Hatala, M.; Vojs, M.; Marton, M.; Matvieiev, O.; Janíková, L.; Chýlková, J. Novel screen-printed sensors with chemically deposited boron-doped diamond and their use for voltammetric determination of attention deficit hyperactivity disorder medication atomoxetine. *Electrochim. Acta* **2022**, *403*, No. 139642.
(34) Tajik, S.; Beitollahi, H.; Nejad, F. G.; Safaei, M.; Zhang, K.; Van Le, Q.; Varma, R. S.; Jang, H. W.; Shokouhimehr, M. Developments and applications of nanomaterial-based carbon paste electrodes. *RSC Adv.* **2020**, *10*, 21561−21581.
(35) Agnihotri, A. S.; Varghese, A.; Nidhin, M. Transition metal oxides in electrochemical and bio sensing: A state-of-art review. *Appl. Surf. Sci. Adv.* **2021**, *4*, No. 100072.
(36) Keshavananda Prabhu, C. P.; Aralekallu, S.; Sajjan, V. A.; Palanna, M.; Kumar, S.; Sannegowda, L. K. Non-precious cobalt phthalocyanine-embedded iron ore electrocatalysts for hydrogen evolution reactions. *Sustainable Energy Fuels* **2021**, *5*, 1448−1457.
(37) Nemakal, M.; Palanna, M.; Sannegowda, L. K.; Kumar, P. S.; et al. Zinc phthalocyanine anchored magnetite particles: Efficient platform for sensing of thiocyanate. *J. Electroanal. Chem.* **2021**, *895*, No. 115385.
(38) Sakthi Priya, T.; Chen, T. W.; Chen, S. M.; Kokulnathan, T.; Akilarasan, M.; Rwei, S. P.; Yu, J. Hierarchical 3D Snowflake-like Iron Diselenide: A Robust Electrocatalyst for Furaltadone Detection. *Inorg. Chem.* **2023**, *62*, 1437−1446.
(39) Kokulnathan, T.; Vishnuraj, R.; Wang, T. J.; Pullithadathil, B. Multidimensional nanoarchitectures of TiO2/Au nanofibers with O-doped C3N4 nanosheets for electrochemical detection of nitrofurazone. *Appl. Surf. Sci.* **2022**, *604*, No. 154474.
(40) Sakthi Priya, T.; Stanley, M. M.; Chen, T. W.; Chen, S. M.; Kokulnathan, T.; Baby, J. N.; George, M. Boosting the Electrochemical Detection Response Toward Hydroxychloroquine via Tungsten Trioxide Nanorods/Nitrogen-Doped Carbon Nanofiber Nanocomposite. *ACS Appl. Nano Mater.* **2022**, *5*, 18670−18679.
(41) Priya, T. S.; Chen, T. W.; Chen, S. M.; Kokulnathan, T.; Lou, B. S.; Al-Onazi, W. A.; Al-Mohaimeed, A. M.; Elshikh, M. S.; Yu, J. Synthesis of perovskite-type potassium niobate using deep eutectic solvents: A promising electrode material for detection of bisphenol A. *Chemosphere* **2023**, *318*, No. 137948.
(42) Kokulnathan, T.; Wang, T. J.; Ahmed, F.; Alshahrani, T. Hydrothermal synthesis of ZnCr-LDH/tungsten carbide composite: a disposable electrochemical strip for mesalazine analysis. *Chem. Eng. J.* **2023**, *451*, No. 138884.
(43) Kokulnathan, T.; Wang, T. J.; Ahmed, F.; Arshi, N. Fabrication of flower-like nickel cobalt-layered double hydroxide for electrochemical detection of carbendazim. *Surf. Interfaces* **2023**, *36*, No. 102570.
(44) Ahmed, F.; Kokulnathan, T.; Umar, A.; Akbar, S.; Kumar, S.; Shaalan, N. M.; Arshi, N.; Alam, M. G.; Aljaafari, A.; Alshoaibi, A. Zinc Oxide/Phosphorus-Doped Carbon Nitride Composite as Potential Scaffold for Electrochemical Detection of Nitrofurantoin. *Biosensors* **2022**, *12*, 856.
(45) Svancara, I.; Kalcher, K.; Walcarius, A.; Vytras, K. *Electroanalysis with Carbon Paste Electrodes*; CRC Press, 2019.

https://doi.org/10.1021/acsomega.3c01726
ACS Omega 2023, 8, 19006−19015

(46) Ziyatdinova, G.; Gimadutdinova, L. Cerium (IV) and iron (III) oxides nanoparticles based Voltammetric sensor for the sensitive and selective determination of Lipoic acid. *Sensors* **2021**, *21*, 7639.
(47) Ganash, A.; Alshammari, S.; Ganash, E. Development of a Novel Electrochemical Sensor Based on Gold Nanoparticle-Modified Carbon-Paste Electrode for the Detection of Congo Red Dye. *Molecules* **2023**, *28*, 19.
(48) Pwavodi, P. C.; Ozyurt, V. H.; Asir, S.; Ozsoz, M. Electrochemical sensor for determination of various phenolic compounds in wine samples using Fe3O4 nanoparticles modified carbon paste electrode. *Micromachines* **2021**, *12*, 312.
(49) Stanković, D.; Mehmeti, E.; Svorc, L.; Kalcher, K. New electrochemical method for the determination of β-carboline alkaloids, harmalol and harmine, in human urine samples and in Banisteriopsis caapi. *Microchem. J.* **2015**, *118*, 95−100.
(50) Zhang, Z.; Wang, E. *Electrochemical Principles and Methods*; Science Press: Beijing, 2000.
(51) Gosser, D. K. *Cyclic Voltammetry, Simulation and Analysis of Reaction Mechanisms*; Wiley VCH: New York, 1993.
(52) Elgrishi, N.; Rountree, K. J.; McCarthy, B. D.; Rountree, E. S.; Eisenhart, T. T.; Dempsey, J. L. A practical beginner's guide to cyclic voltammetry. *J. Chem. Educ.* **2018**, *95*, 197−206.
(53) Laviron, E. Adsorption, auto inhibition and autocatalysis in polarography and linear potential sweep voltammetry. *J. Electroanal. Chem.* **1974**, *52*, 355−393.
(54) Jouikov, V.; Simonet, J. Electrochemical Reactions of Sulfur Organic Compounds. In *Encyclopedia of Electrochemistry*; 2007.
(55) I.C.H.Q. (R2). *Stability Testing of New Drug Substances and Products*, Proc. Int. Conf. Harmon., Geneva Geneva, 2003,2003.
(56) *Identification and Determination of Impurities in Drugs*; Görög, S., Ed.; Elsevier: Amsterdam, 2000; pp 84−96.
(57) ICH Harmonised Tripartite Guideline, Impurities in New Drug Substances Q3A(R2), Current Step 4 version dated 25 October 2006, 6.
(58) Görög, S. Critical review of reports on impurity and degradation product profiling in the last decade. *TrAC, Trends Anal. Chem.* **2018**, *101*, 2−16.
(59) Olsen, B. A.; Baertschi, S. W. Strategies for Investigation and Control of Process-and Degradation-Related Impurities. In *Separation Science and Technology*; Academic Press, 2004; Vol. 5, pp 89−117.
(60) Jain, D.; Basniwal, P. K. Forced degradation and impurity profiling: recent trends in analytical perspectives. *J. Pharm. Biomed. Anal.* **2013**, *86*, 11−35.
(61) Moffat, A. C.; Osselten, M. D.; Widdop, B. *Clarke's Analysis of Drugs and Poisons in Pharmaceuticals, Body Fluids and Postmortem Material*, 3rd ed.; Pharmaceutical Press: London, UK, 2004, p 1370.

https://doi.org/10.1021/acsomega.3c01726
ACS Omega 2023, 8, 19006−19015